1

Joint Beamforming and Channel Reconfiguration for RIS-Assisted Millimeter Wave Massive MIMO-OFDM Systems

Hanyu Wang, Jun Fang, and Hongbin Li, Fellow, IEEE

Abstract—In this paper, we consider the problem of joint active and passive beamforming for reconfigurable intelligent surface (RIS)-assisted millimeter-wave (mmWave) multiple-inputmultiple-output (MIMO) orthogonal frequency-division multiplexing (OFDM) systems. The objective is to maximize the spectral efficiency by jointly optimizing the RIS's reflection coefficients and the hybrid precoder/combiner at the base station (BS)/mobile station (MS). By resorting to classical hybrid precoder/combiner optimization techniques, this joint beamforming problem can be converted into an optimization concerning only the design of the reflection coefficients. Nevertheless, the objective function of the resulting passive beamforming problem does not have an explicit expression of the reflection coefficients. To address this difficulty, the inherent structure of the effective channel is exploited, based on which an approximation of the truncated singular value decomposition (SVD) of the effective channel is obtained, and a favorable propagation environment can be realized by directly manipulating the singular values of the effective channel. Simulation results show that the proposed method can configure a favorable channel with a small condition number. Moreover, the proposed method presents a clear performance advantage over state-of-the-art algorithms, while with a low computational complexity.

Index Terms—MmWave communications, reconfigurable intelligent surface (RIS), joint active and passive beamforming.

I. INTRODUCTION

Millimeter wave (mmWave) communication is regarded as a promising technology for future cellular networks [1]–[3]. Nevertheless, due to reduced diffraction and high penetration loss, mmWave communication has limited coverage and is vulnerable to blockage by obstacles [4]–[6]. Also, the sparse scattering characteristics of mmWave channels make it difficult to exploit the spatial diversity for simultaneous transmission of multiple data streams. To overcome the above challenges, RIS has been recently introduced to improve the spectral efficiency and coverage of mmWave systems [7]–[10]. RIS

Copyright (c) 2015 IEEE. Personal use of this material is permitted. However, permission to use this material for any other purposes must be obtained from the IEEE by sending a request to pubs-permissions@ieee.org.

Hanyu Wang and Jun Fang are with the National Key Laboratory of Science and Technology on Communications, University of Electronic Science and Technology of China, Chengdu 611731, China, Email: JunFang@uestc.edu.cn Hongbin Li is with the Department of Electrical and Computer Engineering,

Hongbin Li is with the Department of Electrical and Computer Engineering, Stevens Institute of Technology, Hoboken, NJ 07030, USA, E-mail: Hongbin.Li@stevens.edu

This work was supported in part by the National Key R&D Program of China under Grant 2018YFB1801500, and in part by the National Science Foundation of China under Grant 61829103. The work of H. Li was supported in part by the National Science Foundation under Grants ECCS-1923739 and ECCS-2212940.

is a planar meta-surface equipped with a large number of programmable passive reflecting elements. With the aid of a smart controller, each reflecting element can independently reflect the incident signal with a reconfigurable amplitude and phase shift, thus helping realize a favorable propagation channel for high-capacity and robust mmWave links [11]–[16].

A key problem of interest in RIS-assisted mmWave communications is to jointly devise the reflection coefficients and the transmit precoder to optimize the system performance. Such a problem is also referred to as joint active and passive beamforming, and has been extensively studied over the past few years [8], [9], [17]-[31]. Most studies on joint active and passive beamforming, however, focused on single-inputsingle-output (SISO) or multiple-input-single-output (MISO) systems, e.g. [8], [17]–[23], which cannot be straightforwardly extended to MIMO systems. In addition, considering the rich spectrum resources available at the mmWave band, mmWave systems are very likely to operate on wideband channels with frequency selectivity [32]. Therefore it is of practical significance to study joint beamforming for massive MIMO OFDM systems. Specifically, in [29], [30], an alternating optimization-based method was proposed to address the joint beamforming problem for massive MIMO-OFDM systems, in which the transmit precoder and the RIS's reflection coefficients are optimized in an alternating manner. Nevertheless, the optimization of the reflection coefficients is still very involved. To address this difficulty, [29] proposed to alternatively optimize each reflection coefficient, with other reflection coefficients fixed. Such a sequential optimization approach, however, incurs a prohibitively high computational complexity. Another approach [30] addresses this difficulty by finding a lower bound of the objective function and employs a majorization-minimization technique to maximize the lower bound. Optimizing the lower bound, however, may lead to a solution that is far from the optimum. In addition to the AO-based method, a low-complexity joint design method was proposed in [31] for joint beamforming for RIS-assisted massive MIMO-OFDM systems. The basic idea is to align the passive beamforming vector with the dominant path of the reflected channel. Nevertheless, as only the dominant path is utilized, this method does not fully exploit the spatial diversity of the reflected channel, which prevents it from achieving a higher spectral efficiency.

In this paper, we study the problem of joint active and passive beamforming for RIS-assisted mmWave MIMO-OFDM systems, where an RIS is deployed to assist the downlink

transmission from the BS to the MS. Specifically, the objective is to maximize the spectral efficiency by jointly optimizing the RIS's reflection coefficients and the hybrid precoder (combiner) at the BS (MS). By resorting to classical hybrid precoder/combiner optimization techniques, we show that this complicated problem can be converted into an optimization concerning only the design of the reflection coefficients. Nevertheless, the objective function of this passive beamforming problem is a function of the singular values of the effective (or equivalent) channel, which does not have an explicit expression of the reflection coefficients. To address this difficulty, we start by analyzing the geometric model of the effective channel and show that it can serve as a good approximation of the truncated SVD of the effective channel. Thus the singular values of the effective channel can be approximated by the path gains associated with the reflected paths which have an explicit expression of the reflection coefficients. A manifoldbased optimization algorithm is then developed to optimize the reflection coefficients.

A major contribution of this work is that we established an explicit mathematical relationship between the singular values of the effective channel and the reflection coefficients. This enables us to customize a favorable propagation channel with a small condition number by directly manipulating its singular values. Note that the idea of the current work is partially inspired by our previous work [25]. Nevertheless, there are several important distinctions between this work and [25]. Firstly, different from [25] which is concerned with single-carrier narrowband channels, this paper considers the joint beamforming problem with wideband frequency-selective mmWave channels. Secondly, in the current work, we consider a more general scenario where a direct link between the BS and the MS is available. In this case, the problem is more complicated as the effective channel is a sum of the direct channel and the reflected channel, and we will need to determine how many and which reflected paths should be chosen for data transmission before optimizing the passive beamforming vector.

The work [26] also customizes a favorable propagation channel via exploiting the inherent structure of the effective channel. It considers a scenario consisting of multiple spatially distributed RISs. For each RIS, only the dominant path of the corresponding BS-RIS-MS channel is selected for data transmission. Therefore the reflection coefficients of each RIS can be easily determined by simply aligning the passive beamforming vector with the dominant path. Different from [26], our work considers a single RIS scenario. The objective is to carefully devise the reflection coefficients of the RIS such that it can fully exploit the spatial diversity of the cascade channel to improve the spectral efficiency of the system. This leads to a passive beamforming design problem that is more complicated than that in [26].

The rest of the paper is organized as follows. In Section II, the system model and the formulation of the active/passive beamforming problem are discussed. The passive beamforming problem is studied in Section III, where a SVD-approximation-based method is developed. In Section IV, based on the optimized reflection coefficients, the design

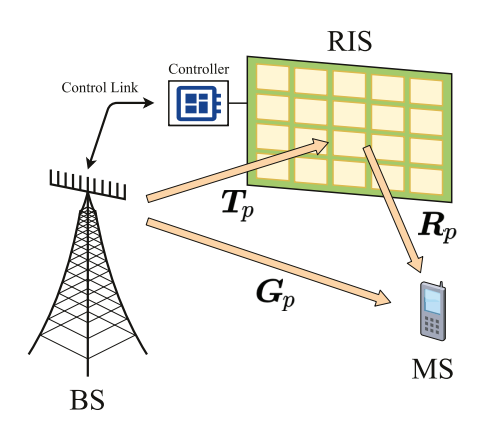


Fig. 1. RIS-assisted MIMO-OFDM downlink communication system..

of active hybrid precoder/combiner is studied. The computational complexity of the proposed method is analyzed in V. Simulation results are presented in Section VI, followed by concluding remarks in Section VII.

Notations: Vectors and matrices are denoted by lowercase and uppercase letters, respectively. \mathbb{R} and \mathbb{C} respectively denote the real space and complex space. The transpose, conjugate, conjugate transpose, Moore-Penrose pseudo inverse, determinant, rank and trace of a matrix X are represented by $X^T, X^*, X^H, X^{\dagger}, \det(X), \operatorname{rank}(X)$ and $\operatorname{tr}(X)$, respectively. The element in the ith row and jth column of X is denoted by X[i,j], while $X[\{i_m\},\{j_n\}]$ denotes the submatrix whose (m, n)th element is equal to (i_m, j_n) th element of X. diag(X)denotes the vector that contains the diagonal elements of X, while diag(x) represents the diagonal matrix that contains the elements of vector x on its main diagonal. $|\cdot|$ and $|\cdot|_F$ indicate the absolute value of a scalar and the Frobenius norm of a matrix, respectively. The real part of a complex number are denoted by $\Re\{\cdot\}$. The identity matrix is denoted by I. The real and complex Gaussian distributions with mean μ and variance σ^2 is denoted by $\mathcal{N}(\mu, \sigma^2)$ and $\mathcal{CN}(\mu, \sigma^2)$, respectively. The Kronecker product and Hadamard product are denoted by \otimes and o, respectively.

II. SYSTEM MODEL AND PROBLEM FORMULATION

A. System Model

Consider a mmWave MIMO-OFDM system, where an RIS is employed to assist data transmission from the BS to the MS as illustrated in Fig. 1. We assume a hybrid analog and digital beamforming structure at both the BS and the MS, in which the BS is equipped with N_t antennas and R_t ($R_t < N_t$) RF chains and the MS is equipped with N_r antennas and R_r ($R_r < N_r$) RF chains. The total number of OFDM tones (subcarriers) is P. For each subcarrier, the BS sends N_s data steams to the MS simultaneously. Specifically, the transmitted signal associated with the pth subcarrier can be expressed as

$$\boldsymbol{z}_p = \boldsymbol{F}_{\mathrm{RF}} \boldsymbol{F}_{\mathrm{BB},p} \boldsymbol{s}_p, \tag{1}$$

where $s_p \in \mathbb{C}^{N_s}$ denotes the pth subcarrier's symbol vector that satisfies $\mathbb{E}\{s_ps_p^H\} = I$, $F_{\mathrm{BB},p} \in \mathbb{C}^{R_t \times N_s}$ is the baseband

precoding matrix associated with pth subcarrier, and $F_{RF} \in \mathbb{C}^{N_t \times R_t}$ is the RF precoding matrix that is common to all subcarriers. Also, we impose a transmit power constraint for each subcarrier, i.e. $\|F_{RF}F_{BB,p}\|_F^2 \leq \rho$.

The procedure to generate the transmitted signal (1) is elaborated as follows. Firstly, the symbol vector s_p at each subcarrier is precoded using a baseband precoding matrix $F_{\mathrm{BB},p}$. The symbol blocks are transformed to the time-domain using P-point inverse discrete Fourier transform (IDFT). A cycle prefix is then added to the symbol block, and finally a common RF precoder F_{RF} is applied to all subcarriers. After the signal received at the MS, a common RF combiner $\mathbf{W}_{\mathrm{RF}} \in \mathbb{C}^{N_r \times R_r}$ is applied to all subcarriers. Then the cyclic prefix is removed and symbols are converted back to the frequency domain by performing a discrete Fourier transform (DFT). Finally, the received signal associated with pth subcarrier is combined using a baseband combining matrix $\mathbf{W}_{\mathrm{BB},p} \in \mathbb{C}^{R_r \times N_s}$. Therefore, the received signal associated with the pth subcarrier can be expressed as

$$\boldsymbol{y}_p = \boldsymbol{W}_{\mathrm{BB},p}^H \boldsymbol{W}_{\mathrm{RF}}^H \boldsymbol{H}_p \boldsymbol{F}_{\mathrm{RF}} \boldsymbol{F}_{\mathrm{BB},p} \boldsymbol{s}_p + \boldsymbol{W}_{\mathrm{BB},p}^H \boldsymbol{W}_{\mathrm{RF}}^H \boldsymbol{n}_p, \quad (2)$$

where $n_p \in \mathbb{C}^{N_r}$ denotes the additive Gaussian noise with zero mean and variance σ^2 , and $H_p \in \mathbb{C}^{N_r \times N_t}$ denotes the frequency-domain channel matrix associated with the pth subcarrier.

The transmitted signal arrives at the receiver via propagating through the direct BS-MS channel and the BS-RIS-MS reflection channel. The RIS is a uniform planar array (UPA) consisting of M reflecting elements, where each of them behaves like a single physical point which combines all the received signals and then re-scatters the combined signal with an adjustable phase shift [19]. Let $G_p \in \mathbb{C}^{N_r \times N_t}$, $T_p \in \mathbb{C}^{M \times N_t}$ and $R_p \in \mathbb{C}^{N_r \times M}$ respectively denote the BS-MS channel, the BS-RIS channel and the RIS-MS channel associated with the pth subcarrier. Also, define

$$\mathbf{\Phi} \triangleq \operatorname{diag}\left(e^{j\phi_1}, \cdots, e^{j\phi_M}\right),\tag{3}$$

where $\phi_m \in [0, 2\pi]$ is the phase shift introduced by the mth passive element of the RIS. Hence, the channel matrix \boldsymbol{H}_p associated with the pth subcarrier can be expressed as

$$\boldsymbol{H}_p = \boldsymbol{G}_p + \boldsymbol{R}_p \boldsymbol{\Phi} \boldsymbol{T}_p. \tag{4}$$

Thus, the achievable spectral efficiency can be expressed as [33]

$$R = \frac{1}{P} \sum_{p=1}^{P} \log_2 \det \left(\boldsymbol{I} + \frac{1}{\sigma^2} (\boldsymbol{W}_{BB,p} \boldsymbol{W}_{RF})^{\dagger} \boldsymbol{H}_p \boldsymbol{F}_{RF} \boldsymbol{F}_{BB,p} \right. \\ \times \boldsymbol{F}_{BB,p}^H \boldsymbol{F}_{RF}^H \boldsymbol{H}_p^H (\boldsymbol{W}_{RF} \boldsymbol{W}_{BB,p}) \right).$$
(5)

B. Channel Model

We adopt the following geometric wideband mmWave channel model to characterize the direct-link channel and the reflection channel. Specifically, the BS-MS channel in the delay domain can be expressed as [32], [34]

$$G(\tau) = \sqrt{\frac{N_r N_t}{L_d}} \sum_{l=1}^{L_d} \tilde{\varrho}_l \mathbf{a}_{MS}(\theta_l^d) \mathbf{a}_{BS}^H(\gamma_l^d) \delta(\tau - \tau_l^d), \quad (6)$$

where $\tilde{\varrho}_l$ is the complex path gain, γ_l^d , θ_l^d and τ_l^d represent the angle of departure (AoD), the angle of arrival (AoA) and the time delay associated with lth path respectively, $a_{\rm BS}(\gamma_l^d)$ and $a_{\rm MS}(\theta_l^d)$ respectively denote the BS's and MS's array response vectors, and $\delta(\cdot)$ represents the Dirac-delta function.

Similarly, the BS-RIS channel $T(\tau)$ and the RIS-MS channel $R(\tau)$ in the delay domain are modeled as

$$T(\tau) = \sqrt{\frac{N_t M}{L_t}} \sum_{l=1}^{L_t} \tilde{\alpha}_l \boldsymbol{a}_{RIS}(\vartheta_{a,l}, \vartheta_{e,l}) \boldsymbol{a}_{BS}^H(\gamma_l) \delta(\tau - \tau_l^t),$$
(7)

$$\boldsymbol{R}(\tau) = \sqrt{\frac{N_r M}{L_r}} \sum_{l=1}^{L_r} \tilde{\beta}_l \boldsymbol{a}_{MS}(\theta_l) \boldsymbol{a}_{RIS}^H(\chi_{a,l}, \chi_{e,l}) \delta(\tau - \tau_l^r),$$
(8)

where $\tilde{\alpha}_l$ ($\hat{\beta}_l$) and τ_l^t (τ_l^r) respectively represent the complex path gain and the time delay, γ_l (θ_l) denotes the AoD (AoA) associated with the BS(MS), $\vartheta_{a,l}$ ($\chi_{a,l}$) and $\vartheta_{e,l}$ ($\chi_{e,l}$) denote the azimuth and elevation AoA (AoD) associated with the RIS, $\boldsymbol{a}_{\text{RIS}}(\vartheta_{a,l},\vartheta_{e,l})$ and $\boldsymbol{a}_{\text{RIS}}(\chi_{a,l},\chi_{e,l})$ denote the RIS's array response vectors.

Accordingly, the frequency-domain channels associated with the pth subcarrier can be respectively written as

$$G_{p} = \sqrt{\frac{N_{r}N_{t}}{L_{d}}} \sum_{l=1}^{L_{d}} \tilde{\varrho}_{l} e^{-j2\pi f_{s}\tau_{l}^{d}\frac{p}{P}} \boldsymbol{a}_{MS}(\theta_{l}^{d}) \boldsymbol{a}_{BS}^{H}(\gamma_{l}^{d}),$$

$$\boldsymbol{T}_{p} = \sqrt{\frac{N_{t}M}{L_{t}}} \sum_{l=1}^{L_{t}} \tilde{\alpha}_{l} e^{-j2\pi f_{s}\tau_{l}^{t}\frac{p}{P}} \boldsymbol{a}_{RIS}(\vartheta_{a,l}, \vartheta_{e,l}) \boldsymbol{a}_{BS}^{H}(\gamma_{l}),$$

$$\boldsymbol{R}_{p} = \sqrt{\frac{N_{r}M}{L_{r}}} \sum_{l=1}^{L_{r}} \tilde{\beta}_{l} e^{-j2\pi f_{s}\tau_{l}^{r}\frac{p}{P}} \boldsymbol{a}_{MS}(\theta_{l}) \boldsymbol{a}_{RIS}^{H}(\chi_{a,l}, \chi_{e,l}),$$

$$(9)$$

where f_s is the sampling frequency.

In the above equations, the normalized array response vectors are defined as follows. For ULA with N antennas, the normalized array response vector is given by

$$\boldsymbol{a}(\gamma) = \frac{1}{\sqrt{N}} [1 \quad \cdots \quad e^{j(n-1)\frac{2\pi d}{\lambda}\sin(\gamma)} \quad \cdots \quad e^{j(N-1)\frac{2\pi d}{\lambda}\sin(\gamma)}]^T,$$
(10)

where d and λ are the antenna spacing and the signal wavelength. For UPA with $M=M_y\times M_z$ antennas, the normalized array response vector is defined as

$$\boldsymbol{a}(\vartheta_a, \vartheta_e) = \frac{1}{\sqrt{M}} \begin{bmatrix} 1 & \cdots & e^{j(M_y - 1)\frac{2\pi d}{\lambda}\sin(\vartheta_a)\cos(\vartheta_e)} \end{bmatrix}^T \\ \otimes \begin{bmatrix} 1 & \cdots & e^{j(M_z - 1)\frac{2\pi d}{\lambda}\sin(\vartheta_e)} \end{bmatrix}^T.$$
(11)

C. Problem Formulation

Our objective is to jointly devise the active hybrid precoder/combiner and the passive beamforming matrix Φ to

maximize the achievable spectral efficiency. The problem can be formulated as

$$\max_{\left\{\substack{\Phi, F_{RF}, \{F_{BB,p}\}_{p=1}^{P}, \\ W_{RF}, \{W_{BB,p}\}_{p=1}^{P}, \}}} \sum_{p=1}^{P} \log_{2} \det \left(\boldsymbol{I} + \frac{1}{\sigma^{2}} (\boldsymbol{W}_{BB,p} \boldsymbol{W}_{RF})^{\dagger} \right) \\
\times \boldsymbol{H}_{p} \boldsymbol{F}_{RF} \boldsymbol{F}_{BB,p} \boldsymbol{F}_{BB,p}^{H} \boldsymbol{F}_{RF}^{H} \boldsymbol{H}_{p}^{H} (\boldsymbol{W}_{RF} \boldsymbol{W}_{BB,p}) \right) \\
\text{s.t.} \quad \|\boldsymbol{F}_{RF} \boldsymbol{F}_{BB,p}\|_{F}^{2} \leq \rho, \forall p = 1, \dots, P, \\
|\boldsymbol{F}_{RF}[i,j]| = |\boldsymbol{W}_{RF}[i,j]| = 1, \forall i, j, \\
\boldsymbol{H}_{p} = \boldsymbol{G}_{p} + \boldsymbol{R}_{p} \boldsymbol{\Phi} \boldsymbol{T}_{p}, \forall p = 1, \dots, P, \\
\boldsymbol{\Phi} = \operatorname{diag}(e^{j\phi_{1}}, \dots, e^{j\phi_{M}}). \tag{12}$$

Note that this work assumes the knowledge of the channel state information (CSI) for joint active and passive beamforming design. Channel estimation for RIS-assisted mmWave systems is an important and challenging task that has been investigated in some works, e.g. [35]–[39].

To simplify the above problem, we first ignore the constraint imposed by the hybrid analog/digital structure and consider a fully digital precoder/combiner. Thus the problem can be simplified as

$$\max_{\{\boldsymbol{\Phi}, \{\boldsymbol{F}_{p}\}, \{\boldsymbol{W}_{p}\}\}} \sum_{p=1}^{P} \log_{2} \det \left(\boldsymbol{I} + \frac{1}{\sigma^{2}} \boldsymbol{W}_{p}^{\dagger} \boldsymbol{H}_{p} \boldsymbol{F}_{p} \boldsymbol{F}_{p}^{H} \boldsymbol{H}_{p}^{H} \boldsymbol{W}_{p}\right)$$
s.t.
$$\|\boldsymbol{F}_{p}\|_{F}^{2} \leq \rho, \forall p = 1, \dots, P,$$

$$\boldsymbol{H}_{p} = \boldsymbol{G}_{p} + \boldsymbol{R}_{p} \boldsymbol{\Phi} \boldsymbol{T}_{p}, \forall p = 1, \dots, P,$$

$$\boldsymbol{\Phi} = \operatorname{diag}(e^{j\phi_{1}}, \dots, e^{j\phi_{M}}).$$
(13)

where $\boldsymbol{F}_p \in \mathbb{C}^{N_t \times N_s}$ and $\boldsymbol{W}_p \in \mathbb{C}^{N_r \times N_s}$ respectively denote the fully digital precoder and combiner associated with pth subcarrier. Once an optimal fully digital precoder/combiner is obtained, a manifold optimization-based method can be utilized to devise the hybrid precoder (combiner) that approximates the optimal fully digital precoder (combiner). Note that such a strategy has been numerically and theoretically justified by previous studies [32], [33], [40], [41].

Given a fixed Φ , we now discuss how to obtain the optimal fully digital precoder and combiner. Suppose $\operatorname{rank}(\boldsymbol{H}_p) \geq N_s$ holds valid for all subcarriers. According to [42], the optimal solution is given as

$$\boldsymbol{F}_{p}^{\star} = \boldsymbol{V}_{p}[:, 1:N_{s}]\boldsymbol{\Lambda}^{1/2}, \quad \boldsymbol{W}_{p}^{\star} = \boldsymbol{U}_{p}[:, 1:N_{s}], \quad (14)$$

where V_p and U_p are obtained via the ordered SVD of the pth subcarrier's channel: $H_p = U_p \Sigma_p V_p^H$, in which Σ_p is a diagonal matrix of singular values, and $\Lambda \in \mathbb{R}^{N_s \times N_s}$ is a diagonal matrix whose diagonal elements are calculated via the water-filling power allocation scheme and Λ satisfies $\operatorname{tr}(\Lambda) = \rho$. Thanks to the massive array gain provided by the RIS and the large number of antennas at the BS, the effective signal-to-noise ratio (SNR) is large, in which case an equal power allocation scheme is near-optimal [40]. Therefore we can approximate F_p^* as:

$$\boldsymbol{F}_{p}^{\star} \approx \sqrt{\frac{\rho}{N_{s}}} \boldsymbol{V}_{p}[:, 1:N_{s}].$$
 (15)

Substituting the optimal precoder/combiner back to (13), we arrive at a problem that only concerns the optimization of the passive reflection matrix Φ :

$$\max_{\mathbf{\Phi}} \quad \sum_{p=1}^{P} \log_2 \det \left(\mathbf{I} + \frac{\rho}{N_s \sigma^2} \bar{\mathbf{\Sigma}}_p^2 \right)$$
s.t.
$$\mathbf{\Phi} = \operatorname{diag}(e^{j\phi_1}, \cdots, e^{j\phi_M}). \tag{16}$$

where $\bar{\Sigma}_p \triangleq \Sigma_p[1:N_s,1:N_s].$

In the following, we will first discuss how to optimize the passive reflection matrix Φ . After the passive reflection matrix is determined, the effective channel matrices $\{H_p\}_{p=1}^P$ can be accordingly calculated, and then the optimal fully digital precoder/combiner can be determined via (14)–(15). Finally, a manifold optimization-based technique can be employed to search for the hybrid analog and digital precoder/combiner to approximate the optimal fully digital precoder/combiner.

III. PROPOSED PASSIVE BEAMFORMING DESIGN METHOD

Note that the singular values in (16) cannot be expressed by Φ in an explicit way. Therefore it is challenging to directly optimize (16). To address this difficulty, we exploit the inherent structure of the effective channels. First, define

$$\varrho_l \triangleq \sqrt{\frac{N_r N_t}{L_d}} \tilde{\varrho}_l \tag{17}$$

$$\alpha_l \triangleq \sqrt{\frac{N_t M}{L_t}} \tilde{\alpha}_l \tag{18}$$

$$\beta_l \triangleq \sqrt{\frac{N_r M}{L_r}} \tilde{\beta}_l \tag{19}$$

For simplicity, we assume that complex path gains are arranged in a decreasing order in terms of magnitude, i.e. $|\rho_1| > \cdots > |\rho_{L_d}|$ ($\{\alpha_l\}$ and $\{\beta_l\}$ are arranged in a similar way). We write the BS-RIS-MS channel as

$$R_{p}\Phi T_{p} = \left(\sum_{m=1}^{L_{r}} \beta_{m} e^{-j2\pi f_{s}\tau_{m}^{r}\frac{p}{P}} \mathbf{a}_{MS}(\theta_{m}) \mathbf{a}_{RIS}^{H}(\chi_{a,m}, \chi_{e,m})\right) \Phi$$

$$\times \left(\sum_{n=1}^{L_{t}} \alpha_{n} e^{-j2\pi f_{s}\tau_{n}^{t}\frac{p}{P}} \mathbf{a}_{RIS}(\vartheta_{a,n}, \vartheta_{e,n}) \mathbf{a}_{BS}^{H}(\gamma_{n})\right)$$

$$= \sum_{m=1}^{L_{r}} \sum_{n=1}^{L_{t}} \beta_{m} \alpha_{n} e^{-j2\pi f_{s}(\tau_{m}^{r} + \tau_{n}^{t})\frac{p}{P}} \mathbf{a}_{MS}(\theta_{m})$$

$$\times \underbrace{\mathbf{a}_{RIS}^{H}(\chi_{a,m}, \chi_{e,m}) \Phi \mathbf{a}_{RIS}(\vartheta_{a,n}, \vartheta_{e,n})}_{d_{mn}} \mathbf{a}_{BS}^{H}(\gamma_{n})$$

$$= \sum_{m=1}^{L_{r}} \sum_{n=1}^{L_{t}} \beta_{m} \alpha_{n} e^{-j2\pi f_{s}(\tau_{m}^{r} + \tau_{n}^{t})\frac{p}{P}} d_{mn} \mathbf{a}_{MS}(\theta_{m}) \mathbf{a}_{BS}^{H}(\gamma_{n})$$

$$= \mathbf{A}_{MS} \mathbf{D}_{p} \mathbf{A}_{BS}^{H}, \tag{20}$$

where

$$\mathbf{A}_{\mathrm{MS}} \triangleq [\mathbf{a}_{\mathrm{MS}}(\theta_1) \cdots \mathbf{a}_{\mathrm{MS}}(\theta_{L_r})],$$
 (21)

$$\mathbf{A}_{\mathrm{BS}} \triangleq [\mathbf{a}_{\mathrm{BS}}(\gamma_1) \cdots \mathbf{a}_{\mathrm{BS}}(\gamma_{L_*})],$$
 (22)

and D_p is an $L_r \times L_t$ matrix with its (m, n)th entry given by

$$\boldsymbol{D}_{p}[m,n] = d_{mn}\beta_{m}\alpha_{n}e^{-j2\pi f_{s}(\tau_{m}^{r} + \tau_{n}^{t})\frac{p}{P}}$$
 (23)

in which d_{mn} is defined as

$$d_{mn} \triangleq \boldsymbol{a}_{RIS}^{H}(\chi_{a,m}, \chi_{e,m}) \boldsymbol{\Phi} \boldsymbol{a}_{RIS}(\vartheta_{a,n}, \vartheta_{e,n})$$

$$= \boldsymbol{v}^{H} \left(\boldsymbol{a}_{RIS}^{*}(\chi_{a,m}, \chi_{e,m}) \circ \boldsymbol{a}_{RIS}(\vartheta_{a,n}, \vartheta_{e,n}) \right)$$

$$= \boldsymbol{v}^{H} \boldsymbol{p}^{mn}, \tag{24}$$

Here $\boldsymbol{v} \triangleq \operatorname{diag}(\boldsymbol{\Phi}^H)$ and $\boldsymbol{p}^{mn} \triangleq \boldsymbol{a}_{\mathrm{RIS}}(\chi_{a,m},\chi_{e,m}) \circ \boldsymbol{a}_{\mathrm{RIS}}(\vartheta_{a,n},\vartheta_{e,n})$.

Thus, we can rewrite the overall effective channel H_p as

$$H_{p} = G_{p} + R_{p}\Phi T_{p}$$

$$= \bar{A}_{MS}\bar{D}_{p}\bar{A}_{BS}^{H} = \bar{A}_{MS}\begin{bmatrix} D_{p} & \mathbf{0} \\ \mathbf{0} & D_{p}^{d} \end{bmatrix}\bar{A}_{BS}^{H}, \tag{25}$$

where

$$\bar{\boldsymbol{A}}_{\mathrm{MS}} \triangleq [\boldsymbol{a}_{\mathrm{MS}}(\theta_1) \cdots \boldsymbol{a}_{\mathrm{MS}}(\theta_{L_r}) \ \boldsymbol{a}_{\mathrm{MS}}(\theta_1^d) \cdots \boldsymbol{a}_{\mathrm{MS}}(\theta_{L_d}^d)],$$
(26)

$$\bar{\boldsymbol{A}}_{\mathrm{BS}} \triangleq [\boldsymbol{a}_{\mathrm{BS}}(\gamma_1) \cdots \boldsymbol{a}_{\mathrm{BS}}(\gamma_{L_t}) \ \boldsymbol{a}_{\mathrm{BS}}(\gamma_1^d) \cdots \boldsymbol{a}_{\mathrm{BS}}(\gamma_{L_d}^d)],$$
(27)

$$\boldsymbol{D}_{p}^{d} \triangleq \operatorname{diag}(\varrho_{1}e^{-j2\pi f_{s}\tau_{l}^{d}\frac{p}{P}}, \cdots, \varrho_{L_{d}}e^{-j2\pi f_{s}\tau_{l}^{d}\frac{p}{P}}). \tag{28}$$

It can be easily verified that

$$|\boldsymbol{a}(\gamma_i)^H \boldsymbol{a}(\gamma_j)| \to 0, \quad N \to \infty,$$
 (29)

for any $\sin(\gamma_i) \neq \sin(\gamma_j)$. Therefore for sufficiently large values of N_t and N_r , $\bar{A}_{\rm MS}$ and $\bar{A}_{\rm BS}$ can be treated as orthonormal matrices in which the column vectors form an orthonormal set. Also, as shown in [25], if the passive beamforming vector \boldsymbol{v} is optimized to maximize $\{|d_{m,m}|\}$, i.e. the magnitude of diagonal entries of \boldsymbol{D}_p , the optimized \boldsymbol{v} will be approximately orthogonal to \boldsymbol{p}^{mn} , $\forall m \neq n$, thus leading to a quasi-diagonal matrix \boldsymbol{D}_p with negligible off-diagonal entries. Inspired by this fact, we can treat $\bar{\boldsymbol{A}}_{\rm MS}\bar{\boldsymbol{D}}_p\bar{\boldsymbol{A}}_{\rm BS}^H$ as an approximation of the truncated SVD of the effective channel \boldsymbol{H}_p .

Without loss of generality, we assume that the top N_s singular values of \boldsymbol{H}_p comprise of two subsets, namely, $\{d_{R,k}^{(p)}\}_{k=1}^K$ that are the top K (in terms of magnitude) diagonal entries of \boldsymbol{D}_p and $\{d_{D,k}^{(p)}\}_{k=1}^{K'}$ that are the top K' (in terms of magnitude) diagonal entries of \boldsymbol{D}_p^d , where we have $K+K'=N_s$ and

$$d_{R,k}^{(p)} \triangleq \mathbf{D}_p[i_k, i_k], \ \forall k = 1, \cdots, K,$$
 (30)

$$d_{D,k}^{(p)} \triangleq \boldsymbol{D}_p^d[k,k], \ \forall k = 1, \cdots, N_s - K.$$
 (31)

Note that the selection indices, $\{i_k\}$ and $\{k\}$, are the same for different subcarriers as the magnitudes of diagonal entries of D_p and D_p^d ,

$$|\boldsymbol{D}_{p}[i,i]| = |\boldsymbol{v}^{H}\boldsymbol{p}^{ii}||\beta_{i}\alpha_{i}|, \ \forall i = 1, \cdots, \min(L_{t}, L_{r}), \ (32)$$

$$|\boldsymbol{D}_{p}^{d}[i,i]| = |\varrho_{i}|, \ \forall i = 1, \cdots, L_{d}, \tag{33}$$

are both independent of the subcarrier index p. Therefore, the truncated singular value matrix of \boldsymbol{H}_p , $\bar{\boldsymbol{\Sigma}}_p$, can be approximated as

$$\hat{\Sigma}_{p} = \operatorname{diag}\left(d_{R,1}^{(p)}, d_{R,2}^{(p)}, \cdots, d_{R,K}^{(p)}, d_{D,1}^{(p)}, d_{D,2}^{(p)}, \cdots, d_{D,N_{s}-K}^{(p)}\right).$$
(34)

Substituting $\{\hat{\bar{\Sigma}}_p\}_{p=1}^P$ into the objective function of (16), we have

$$\sum_{p=1}^{P} \log_{2} \det \left(\mathbf{I} + \frac{\rho}{N_{s}\sigma^{2}} \hat{\mathbf{\Sigma}}_{p}^{2} \right)$$

$$= \sum_{p=1}^{P} \left\{ \sum_{k=1}^{K} \log_{2} \left(1 + \frac{\rho}{N_{s}\sigma^{2}} \left| d_{R,k}^{(p)} \right|^{2} \right) + \sum_{k=1}^{N_{s}-K} \log_{2} \left(1 + \frac{\rho}{N_{s}\sigma^{2}} \left| d_{D,k}^{(p)} \right|^{2} \right) \right\}$$

$$= P \left\{ \sum_{k=1}^{K} \log_{2} \left(1 + \frac{\rho |\beta_{i_{k}} \alpha_{i_{k}}|^{2}}{N_{s}\sigma^{2}} \left| \mathbf{v}^{H} \mathbf{p}^{i_{k}i_{k}} \right|^{2} \right) + \sum_{i=1}^{N_{s}-K} \log_{2} \left(1 + \frac{\rho |\varrho_{i}|^{2}}{N_{s}\sigma^{2}} \right) \right\}.$$
(35)

Therefore the optimization (16) can be re-expressed as

$$\max_{\boldsymbol{v},\{i_{k}\}_{k=1}^{K}} \sum_{k=1}^{K} \log_{2} \left(1 + a_{i_{k}} | \boldsymbol{v}^{H} \boldsymbol{p}^{i_{k}i_{k}} |^{2} \right) + R_{D}(N_{s} - K)$$
s.t. $\boldsymbol{v} = [e^{j\phi_{1}} \cdots e^{j\phi_{M}}]^{H}, K \leq N_{s}.$ (36)

where $a_i \triangleq \frac{\rho |\beta_i \alpha_i|^2}{N \sigma^2}$ and

$$R_D(n) \triangleq \sum_{i=1}^n \log_2 \left(1 + \rho |\varrho_i|^2 / (N_s \sigma^2) \right). \tag{37}$$

To simplify the problem, we first suppose K is pre-specified. In this case, the second term in the above optimization becomes a constant. Hence we only need to jointly optimize v and the index set $\{i_k\}_{k=1}^K$ to maximize the spectral efficiency:

$$\max_{\boldsymbol{v},\{i_k\}_{k=1}^K} \quad \sum_{k=1}^K \log_2 \left(1 + a_{i_k} | \boldsymbol{v}^H \boldsymbol{p}^{i_k i_k} |^2 \right)
\text{s.t.} \quad \boldsymbol{v} = [e^{j\phi_1} \cdots e^{j\phi_M}]^H$$
(38)

A. Determining The Index Set $\{i_k\}_{k=1}^K$ and The Value K

To gain insight into the above optimization problem, notice that the vector \boldsymbol{p}^{ij} , which is defined as the Hadamard product of two steering vectors, i.e. $\boldsymbol{p}^{ij} \triangleq \boldsymbol{a}_{\mathrm{RIS}}(\chi_{a,i},\chi_{e,i}) \circ \boldsymbol{a}_{\mathrm{RIS}}(\vartheta_{a,j},\vartheta_{e,j})$, is asymptotically orthogonal to \boldsymbol{p}^{mn} for any $i \neq m$ or $j \neq n$. This fact inspires us to construct an orthonormal matrix $\boldsymbol{P} \in \mathbb{C}^{M \times M}$, in which its first $L_r L_t$ columns are $\{\bar{\boldsymbol{p}}^{ij} \triangleq \sqrt{M} \boldsymbol{p}^{ij}\}_{i=1,j=1}^{L_t,L_r}$ and the rest $M-L_r L_t$ columns, denoted by $\{\boldsymbol{q}_i\}$, form an orthonormal set that are orthogonal to the first $L_r L_t$ columns. Here the scaling factor \sqrt{M} is used to ensure $\sqrt{M} \boldsymbol{p}^{ij}$ has unit norm. We can now express \boldsymbol{v} as

$$v = Pc = \sum_{m=1}^{L_t} \sum_{n=1}^{L_r} c_{(m-1)L_r + n} \bar{p}^{mn} + \sum_{i=1}^{M-L_t L_r} c_{L_t L_r + i} q_i$$
(39)

Meanwhile, the following holds

$$M = \mathbf{v}^H \mathbf{v} = \sum_{m=1}^{L_t} \sum_{n=1}^{L_r} |c_{(m-1)L_r+n}|^2 + \sum_{i=1}^{M-L_t L_r} |c_{L_t L_r+i}|^2$$
(40)

Substituting (39) into (38) and ignoring the unit-modulus constraint placed on v, we arrive at

$$\max_{\{c_i\},\{i_k\}_{k=1}^K} \sum_{k=1}^K \log_2 \left(1 + \frac{a_{i_k}}{M} |c_{(i_k-1)L_r + i_k}|^2 \right)$$
s.t.
$$\sum_{i=1}^M |c_i|^2 \le M.$$
(41)

Since we have $a_1 \geq \cdots \geq a_{N_s}$, choosing $\{i_k\} = \{1, \cdots, K\}$ can achieve a maximum objective function value, in which case c_j should be set to zero except for those K entries $\{c_{(i-1)L_r+i}\}_{i=1}^K$. In fact, due to the massive array gain provided by the RIS, for those nonzero entries, an equal power allocation scheme is near-optimal, i.e., we have $|c_{(i-1)L_r+i}|^2 = \frac{M}{K}, \forall i=1,\ldots,K$, in which case the above objective function value is equal to $\sum_{i=1}^K \log_2(1+a_i/K)$.

We now discuss how to determine the value of K. Based on the above analysis, the problem (36) can be simplified as

$$\max_{K} \sum_{i=1}^{K} \log_2 \left(1 + \frac{a_i}{K} \right) + R_D(N_s - K)$$
s.t. $K \le N_s$. (42)

Thus the optimal K^* can be obtained via a simple exhaustive search as the object function value can be easily calculated.

B. Manifold-based Method for Passive Beamforming Design

Since the optimal index set $\{i_k\} = \{1, \dots, K^*\}$ has been determined, we see that $R_D(N_s - K^*)$ is a constant and the optimization (36) can be simplified as

$$\max_{\boldsymbol{v}} \quad \sum_{i=1}^{K^{\star}} \log_2 \left(1 + a_i \boldsymbol{v}^H \boldsymbol{P}_i \boldsymbol{v} \right)$$
s.t. $\boldsymbol{v} = [e^{j\phi_1} \cdots e^{j\phi_M}]^H$. (43)

where $P_i \triangleq p^{ii}(p^{ii})^H$. To achieve a good balance between the computational complexity and the performance, a manifold-based method can be employed to solve the passive beamforming design problem.

Specifically, for the optimization (43), the search space can be regarded as a submanifold of \mathbb{C}^M , which is known as the *complex circle manifold* (CCM) [43] and defined as

$$\mathcal{M} = \mathcal{S}^M \triangleq \{ \boldsymbol{u} \in \mathbb{C}^M : |u_i| = 1, i = 1, 2, \cdots M \}. \tag{44}$$

The tangent space that consists of all tangent vectors to $\mathcal M$ at the point v^t can be expressed as

$$\mathcal{T}_{v^t}\mathcal{M} = \{ \boldsymbol{z} \in \mathbb{C}^M : \Re\{\boldsymbol{z} \circ (\boldsymbol{v}^t)^*\} = \boldsymbol{0} \}. \tag{45}$$

Since the descent is performed on the manifold, we need to find the direction of the greatest decrease from the tangent space, which is known as the negative Riemannian gradient. It can be readily verified that the *Riemannian gradient* of the objective function $f(\boldsymbol{v}) \triangleq -\sum_{i=1}^{K^*} \log_2 \left(1 + a_i \boldsymbol{v}^H \boldsymbol{P}_i \boldsymbol{v}\right)$ is given by [43]:

$$\nabla f_{\mathcal{M}}(\boldsymbol{v}^{t}) = \operatorname{Proj}_{\mathcal{T}_{\boldsymbol{v}^{t}}\mathcal{M}} \left(\nabla f(\boldsymbol{v}^{t}) \right)$$

$$= \nabla f(\boldsymbol{v}^{t}) - \mathfrak{R} \{ \nabla f(\boldsymbol{v}^{t}) \circ (\boldsymbol{v}^{t})^{*} \} \circ \boldsymbol{v}^{t},$$
(46)

Algorithm 1 Proposed Passive Beamforming Design Algorithm

- 1: Input channel state information, number of data streams N_s ;
- 2: **for** $K = 0, 1, \dots, N_s$ **do**
- 3: Calculate the objective function value of (42);
- 4: end for
- 5: Determine K^* as the K that achieves the maximum objective function value;
- 6: Initialize $v^0 \in \mathcal{M}$ and select a pre-defined threshold ϵ ;
- 7: repeat
- 8: Calculate the Euclidean gradient $\nabla f(v^t)$ via (47);
- 9: Calculate the Riemannian gradient $\nabla f_{\mathcal{M}}(\mathbf{v}^t)$ via (46);
- 10: Choose an Armijo step size ϖ^t as shown in [44];
- 11: Update \bar{v}^t on the tangent space via (48);
- 12: Update v^{t+1} via mapping v^t onto the complex circle manifold as shown in (49);
- 13: **until** the gap of the objective function values of f(v) between two iterations is smaller than ϵ
- 14: Output the optimal reflecting vector $v^{\star} = v^{t+1}$.

where $\text{Proj}(\cdot)$ is the orthogonal projection operator and the Euclidean gradient $\nabla f(v^t)$ is given as

$$\nabla f(\boldsymbol{v}^t) = -\sum_{i=1}^{K^*} \frac{1}{\ln 2} \frac{2a_i \boldsymbol{P}_i \boldsymbol{v}^t}{1 + a_i (\boldsymbol{v}^t)^H \boldsymbol{P}_i \boldsymbol{v}^t}.$$
 (47)

Next, the gradient decent method is utilized to update \boldsymbol{v}^t on the tangent space as

$$\bar{\boldsymbol{v}}^t = \boldsymbol{v}^t - \varpi^t \nabla f_{\mathcal{M}}(\boldsymbol{v}^t). \tag{48}$$

where ϖ^t is chosen as the Armijo step size [44]. Finally, the retraction operator is performed to map the point on the tangent space onto complex circle manifold \mathcal{M} :

$$\boldsymbol{v}^{t+1} = R(\bar{\boldsymbol{v}}^t) \triangleq \bar{\boldsymbol{v}}^t \circ \left[\frac{1}{|\bar{v}_1^t|}, \cdots, \frac{1}{|\bar{v}_M^t|}\right]^T.$$
 (49)

where \bar{v}_m^t denotes the mth element of \bar{v}^t . Therefore, by iteratively updating (48) and (49) until the gap of the objective function between two iterations attains a small value, an effective solution of v^\star can be obtained. For clarity, The above algorithm is summarized in Algorithm 1.

C. Convergence Analysis

To analyze the convergence of Algorithm 1, we refer to the following theorem given in [45].

Theorem 1: For an optimization problem defined on compact Riemannian manifold \mathcal{M} , i.e.

$$\min_{\boldsymbol{v} \in \mathcal{M}} f(\boldsymbol{v}),\tag{50}$$

if the objective function is bounded below on \mathcal{M} , i.e. $f(v) > -\infty, \forall v \in \mathcal{M}$, and f(v) has locally Lipschitz continuous gradient in Euclidean space, the Riemannian gradient descent method with backtracking Armijo line-search can sufficiently returns a point $v^{(t+1)}$ that satisfies $f(v^{(t+1)}) \leq f(v^{(t)})$ with $\|\nabla f_{\mathcal{M}}(v_t)\| \leq \epsilon_0$ in $\mathcal{O}(1/\epsilon_0^2)$ iterations.

It can be easily verified that for our optimization problem, its objective function is bounded below on \mathcal{M} . Meanwhile, the norm of the Hessian matrix is obviously locally bounded and therefore the objective function has locally Lipschitz continuous gradient in Euclidean space. Thus, the convergence of the proposed passive beamforming algorithm can be guaranteed.

IV. HYBRID PRECODING/COMBINING DESIGN

After the passive beamforming matrix $\Phi^* = \operatorname{diag}((v^*)^H)$ is optimized, the effective channel associated with each subcarrier, i.e. $H_p = G_p + R_p \Phi T_p$, $\forall p$ can be accordingly determined. Hence the optimal fully-digital precoder and combiner, $\boldsymbol{F}_{p}^{\star}$ and $\boldsymbol{W}_{p}^{\star}$, associated with the pth subcarrier can be obtained via a truncated SVD of the effective channel H_p , as showed in (14). Since a hybrid beamforming/combining structure is employed, we need to design a common analog precoding (combining) matrix F_{RF} (W_{RF}) and a set of baseband precoding (combining) matrices for different subcarriers $\{F_{{\rm BB},p}\}$ $(\{{m W}_{{
m BB},p}\})$ to approximate $\{{m F}_p^{\star}\}(\{{m W}_p^{\star}\})$. Such a problem can be formulated as

$$\min_{\substack{\boldsymbol{F}_{RF}, \{\boldsymbol{F}_{BB,p}\}_{p=1}^{P} \\ \text{s.t.}}} \sum_{p=1}^{P} \|\boldsymbol{F}_{p}^{\star} - \boldsymbol{F}_{RF} \boldsymbol{F}_{BB,p}\|_{F}^{2} \\
\text{s.t.} \quad |\boldsymbol{F}_{RF}[i,j]| = 1, \forall i, j. \tag{51}$$

$$\min_{\mathbf{W}_{RF}, \{\mathbf{W}_{BB,p}\}_{p=1}^{P}} \sum_{p=1}^{P} \|\mathbf{W}_{p}^{\star} - \mathbf{W}_{RF} \mathbf{W}_{BB,p}\|_{F}^{2}
\text{s.t.} \quad |\mathbf{W}_{RF}[i,j]| = 1, \forall i, j.$$
(52)

Let

$$F^{\star} \triangleq [F_{1}^{\star}, \cdots, F_{P}^{\star}],$$

$$W^{\star} \triangleq [W_{1}^{\star}, \cdots, W_{P}^{\star}],$$

$$F_{BB} \triangleq [F_{BB,1}, \cdots, F_{BB,P}],$$

$$W_{BB} \triangleq [W_{BB,1}, \cdots, W_{BB,P}],$$
(53)

The problem can be formulated as

$$\min_{\boldsymbol{f} \in \mathcal{M}_f, \boldsymbol{F}_{BB}} \| \boldsymbol{F}^* - \boldsymbol{F}_{RF} \boldsymbol{F}_{BB} \|_F^2,
\min_{\boldsymbol{w} \in \mathcal{M}_w, \boldsymbol{W}_{BB}} \| \boldsymbol{W}^* - \boldsymbol{W}_{RF} \boldsymbol{W}_{BB} \|_F^2, \tag{54}$$

where $f \triangleq \text{vec}(F_{\text{RF}})$, $w \triangleq \text{vec}(W_{\text{RF}})$ and the search space are complex circle manifold defined as $\mathcal{M}_f \triangleq \mathcal{S}^{N_t R_t}$, $\mathcal{M}_w \triangleq$ $\mathcal{S}^{N_rR_r}$. Similarly, a manifold search algorithm [46] can be utilized to solve (54), where we optimize $F_{\rm RF}$ ($W_{\rm RF}$) and $F_{\rm BB}$ ($W_{\rm BB}$) in an alternating manner. The detailed procedure can be found in [46] and thus omitted here. For clarity, the proposed algorithm is summarized in Algorithm 2.

V. COMPUTATIONAL COMPLEXITY ANALYSIS

We now analyze the computational complexity of our proposed joint beamforming design algorithm as summarized in Algorithm 2. Specifically, our proposed method proceeds in two steps. The first step is to solve the passive beamforming problem whose objective is to optimize the RIS's reflection coefficients. In this step, a manifold-based method is employed Algorithm 2 Proposed Joint Beamforming Algorithm

Input: $\{G_p\}_{p=1}^P$, $\{T_p\}_{p=1}^P$, $\{R_p\}_{p=1}^P$, R_t , R_r , N_s , ρ , σ^2 .

1: Optimize the RIS's reflection coefficients Φ^* $diag((\boldsymbol{v}^{\star})^{H})$ via Algorithm 1;

- 2: Compute the effective channel $\boldsymbol{H}_p =$ $\mathbf{R}_p \mathbf{\Phi}^* \mathbf{T}_p, \forall p = 1, \cdots, P;$
- 3: Obtain optimal precoding and combining matrices, i.e. F_n^{\star} and W_p^* , via (14) for $p = 1, \dots, P$;
- 4: Obtain hybrid precoding and combining matrices, i.e.

to solve the passive beamforming problem. The dominant operation for the manifold-based algorithm is to calculate the Riemannian and Euclidean gradient (46)-(47), which has a computational complexity at the order of $\mathcal{O}(M)$. Let I_1 denotes the number of iterations required to converge, the first step involves a computational complexity of $\mathcal{O}(MI_1)$. Given fixed reflection coefficients, the second step aims to search for the optimal hybrid precoding and combining matrices used by the transceiver. To obtain the optimal precoder/combiner, we need to compute the SVD of the effective channel for each subcarrier, which has a computational complexity in the order of $\mathcal{O}(PN_rN_t\min(N_r,N_t))$. After that, a manifoldbased algorithm is employed to search for a common analog precoding (combining) matrix and subcarrier-dependent baseband precoding (combining) matrices to approximate the optimal precoder (combiner). It can be readily verified that this task involves a computational complexity in the order of $\mathcal{O}(PN_rI_2+PN_tI_2)$, where I_2 denotes the number of iterations required to converge. Therefore, the overall computational complexity of our proposed algorithm is in the order of $\mathcal{O}(MI_1 + PN_rN_t\min(N_r, N_t) + PN_rI_2 + PN_tI_2).$

For comparison, we consider two state-of-the-art methods, the alternating optimization (AO)-based algorithm [29], [30] which alternatively optimizes the precoding matrix and RIS's reflecting coefficients, and the simple joint design (SJD) method [31] whose basic idea is to set the RIS coefficients to align the dominant path of the BS-RIS-MS channel. To reduce the computational complexity of the AO algorithm, the majorization-minimization (MM) technique proposed in [30] is considered in our experiments, and the method is termed as "AO-MM". Let I_{AO} and I_{MM} denote the number of iterations required for the AO scheme and the MM technique, respectively. To provide a better comparison of these methods, we suppose $N_t \geq N_r, N_r \gg R_r = R_t \geq N_s$, and $M \gg L_d = L_t = L_r$, which is a reasonable setup for practical mmWave systems. The computational complexity of respective algorithms is summarized in Table I. We see that our proposed method has a lower complexity than the AO-based method.

VI. SIMULATION RESULTS

We now present simulation results to illustrate the performance of our proposed algorithm. In our simulations, we consider a three-dimensional setup as shown in Fig. 2. The

TABLE I

COMPUTATIONAL COMPLEXITY COMPARISON

Algorithm	Dominant computational complexity
Proposed method	$\mathcal{O}(MI_1 + PN_tN_r^2)$
AO-MM method	$\mathcal{O}\left((M^3 + M^2 I_{\text{MM}} + P N_t N_r^2) I_{\text{AO}}\right)$
SJD method	$\mathcal{O}(M + PN_tN_r)$

coordinates of the BS, the RIS and the MS are respectively set as $(x_{\rm BS}, 0, z_{\rm BS})$, $(0, y_{\rm RIS}, z_{\rm RIS})$, and $(x_{\rm MS}, y_{\rm MS}, z_{\rm MS})$, where we set $x_{\rm BS}=2$ m, $z_{\rm BS}=10$ m, $y_{\rm RIS}=148$ m, $z_{\rm RIS}=10$ m, $x_{\rm MS}=5$ m, $y_{\rm MS}=150$ m, and $z_{\rm MS}=1.5$ m. The distance-dependent path loss is modeled as

$$\kappa = a + 10b \log_{10}(\tilde{d}) + \xi, \tag{55}$$

where \tilde{d} denotes the distance between the transmitter and the receiver, and $\xi \sim \mathcal{N}(0, \sigma_{\xi}^2)$.

Slightly different from our previous definition, the effective channel is modeled as follows by considering the transmitter and receiver antenna gains [47]

$$\boldsymbol{H}_{p} = G_{t}G_{r}\left(\boldsymbol{G}_{p} + \boldsymbol{R}_{p}\boldsymbol{\Phi}\boldsymbol{T}_{p}\right),\tag{56}$$

where G_t and G_r represent the BS's and MS's antenna gains, respectively. For the BS-RIS channel T_p and the RIS-MS channel R_p , the gain of the LOS path is assumed to follow a complex Gaussian distribution $\tilde{\alpha}_1(\tilde{\beta}_1) \sim \mathcal{CN}(0, -10^{-0.1\kappa}),$ in which κ is calculated according to (55) and we set a =61.4, b=2, and $\sigma_{\xi}=5.8 \text{dB}$ as suggested by LOS realworld channel measurements [48]. On the other hand, the gain of the NLOS paths is assumed to follow $\tilde{\alpha}_i(\beta_i) \sim$ $\mathcal{CN}(0, -10^{-0.1(\kappa+\mu)})$, where μ is the Rician factor [49]. As for the BS-MS channel G_p , the path gain is assumed to follow $\tilde{\varrho}_i \sim \mathcal{CN}(0,-10^{-0.1(\kappa+\delta)})$, in which κ is calculated by setting $a=72,\,b=2.92,$ and $\sigma_{\xi}=8.7\text{dB},$ as suggested by NLOS real-world channel measurements [48], and each path is assumed to pass through tintedglass walls with an additional penetration loss $\delta = 40.1 \text{dB}$ [50]. The delay spread τ for each path is independently generated and follows a uniform distribution.

Unless otherwise specified, we assume that the RIS employs a UPA with $M=M_y\times M_z=16\times 16$ passive elements, the BS and the MS adopt ULAs with $N_t=16$ and $N_r=16$ antennas. Other parameters are set as follows: P=16, $R_t=R_r=8$, $N_s=6$, $L_t=L_r=L_d=8$, $G_t=24.5 {\rm dBi}$, $G_r=0 {\rm dBi}$, $f_s=2 {\rm GHz}$. The central carrier frequency is set to 28GHz, the bandwidth of subcarrier is set to 250MHz and thus the noise power is $\sigma^2=-174+10\log_{10}B=-90 {\rm dBm}$.

We compare our proposed method with the following two algorithms, namely, the alternating optimization (AO)-based algorithm [29], [30] which alternatively optimizes the precoding matrix and RIS's reflecting coefficients, and the simple joint design (SJD) method [31] whose basic idea is to set the RIS coefficients to align the dominant path of the BS-RIS-MS channel. To reduce the computational complexity of the AO algorithm, the majorization-minimization (MM) technique proposed in [30] is considered in our experiments, and the method is termed as "AO-MM". Besides, we also consider the

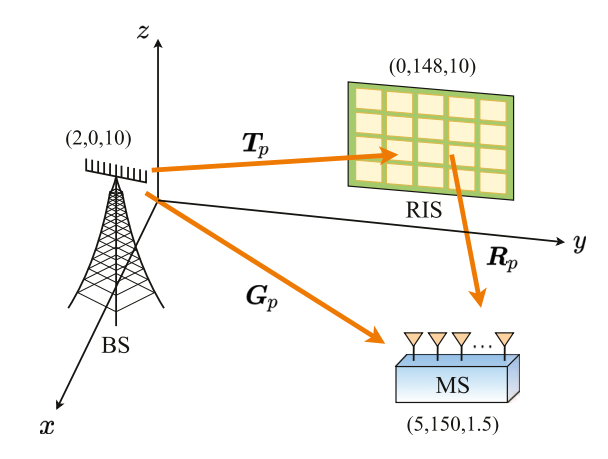


Fig. 2. An illustration of simulation setup.

case when there is no RIS in the system, which is labeled as "No RIS".

Fig. 3 plots the spectral efficiency of respective algorithms versus the transmit power ρ with different Rician factors μ . We see that the RIS-assisted system achieves a significant performance improvement over the system without RIS. Also, our proposed method presents a clear performance advantage over the other two methods as the transmit power increases. This is probably because our proposed method can fully utilize the spatial diversity rendered by the BS-RIS-MS channel. Due to the water-filling power allocation, the spatial diversity can be better utilized when the transmit power is large. In addition, we see that the performance improvement of our proposed method over the other two methods is more pronounced when the Rician factor is set to $\mu=1$ dB. This is because the spatial diversity can be more efficiently utilized for channels with a smaller Rician factor.

Fig. 4 depicts the spectral efficiency of respective algorithms as a function of the number of data streams N_s , where we set $\rho=30 {\rm dBm}$. We can observe that our proposed method outperforms the AO-MM method and the SJD method. Also, the SJD method does not improve as significantly as the other two methods as the number of data streams grows, which is due to the fact that the SJD method only utilizes the dominant path of the BS-RIS-MS channel and fails to fully utilize the spatial diversity rendered by the reflection channel for multiple stream transmission.

In Fig. 5, we report the spectral efficiency of respective algorithms versus the number of reflecting elements M, where we set the transmit power $\rho=30 \mathrm{dBm}$. In Fig. 5, we see that for all algorithms, the spectral efficiency increases as the number of reflection elements increases, and RIS-assisted systems provide a substantial advantage over the no-RIS communication system. Meanwhile, our proposed method outperforms the AO-MM and the SJD method by a big margin. Note that, compared with the AO-MM and the SJD, the performance advantage of our proposed method is more pronounced as M increases. This is because more reflecting elements can improve the gains of the reflected paths, thus

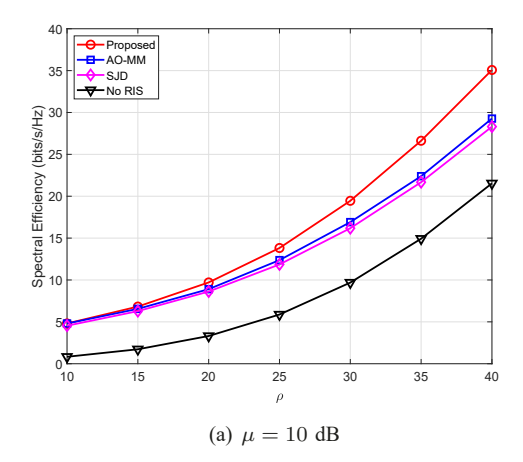


Fig. 3. Spectral efficiency versus the transmit power ρ .

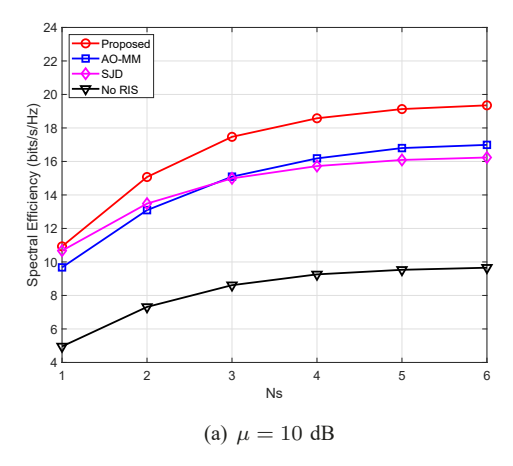


Fig. 4. Spectral efficiency versus the number of data streams N_s .

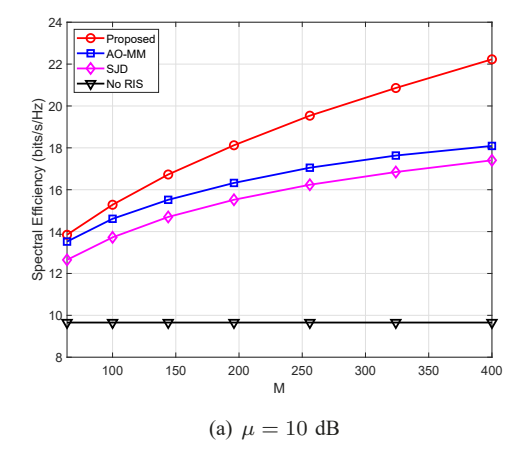
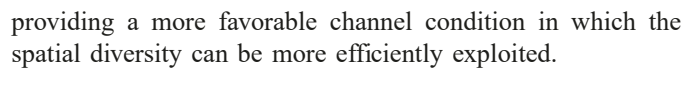
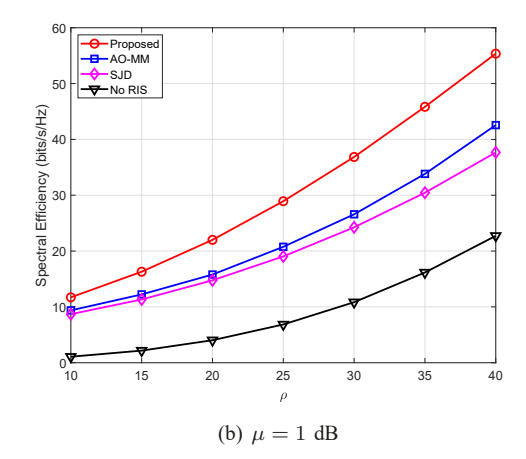
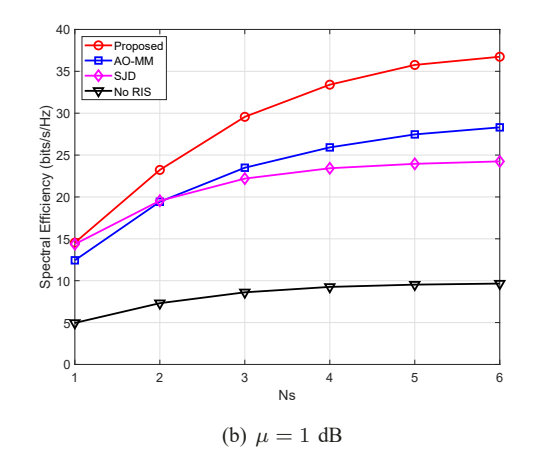


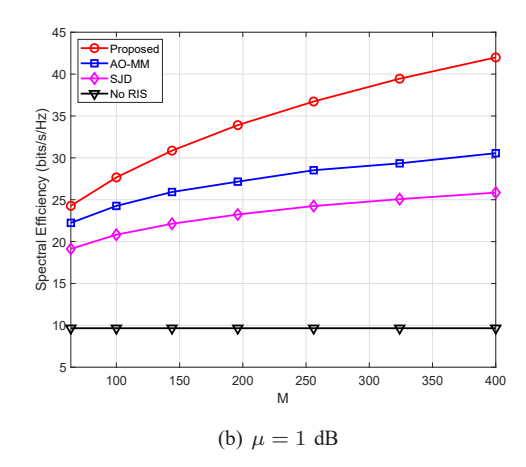
Fig. 5. Spectral efficiency versus the number of RIS elements ${\cal M}.$



In Fig. 6, the average runtimes of respective algorithms are depicted. It can be observed that our proposed method is computationally much more efficient than the AO-MM method. The SJD method has the lowest complexity as its pas-







sive beamforming vector, simply determined by the dominant reflection path, has a simple analytical solution. Nevertheless, as indicated earlier, the SJD method cannot fully exploit the spatial diversity rendered by the reflection channel, and thus suffers a substantial performance loss compared to our proposed method. We also observe that the complexity of our proposed method increases slowly as M grows. Overall, our proposed method can achieve a good balance between the performance and the computational complexity.

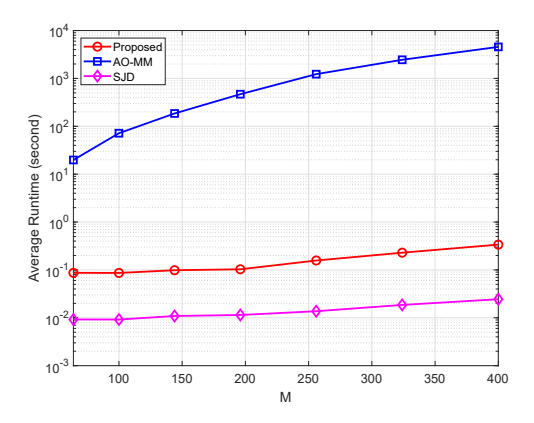


Fig. 6. Average run time versus the number of RIS elements M.

To gain an insight into how the RIS helps realize a favorable propagation environment, we use the truncated condition number as a metric to evaluate the capability of respective algorithms in reconfiguring the wireless channel. The average truncated condition number is defined as $\frac{1}{P}\sum_{p=1}^{P}\frac{|\mathbf{\Sigma}^{(p)}[1,1]|}{|\mathbf{\Sigma}^{(p)}[N_s,N_s]|}$, where $\Sigma^{(p)}[i,i]$ denotes the *i*th largest singular value of the effective channel H_p . It is noted that a smaller truncated condition number indicates a more favorable propagation environment since we prefer the power of the channel to be uniformly distributed over singular values to support multistream transmission. Fig. 7 depicts the truncated condition number of respective algorithms as a function of the number of reflecting elements M, where we set $\rho = 30 \text{dBm}$ and $\mu = 10 \text{dB}$. It can be observed that the truncated condition number of the SJD method grows rapidly as M increases. This is because the SJD method optimizes the RIS's reflection coefficients only to enhance the dominant path of the BS-RIS-MS channel, with other reflected paths neglected. In contrast, the truncated condition number of our proposed method increases slightly with an increasing M, thus creating a more favorable channel for exploiting spatial diversity. We see that the AO-MM method also achieves a condition number similar to our proposed method. Nevertheless, it is observed that the singular values of the effective channel obtained by the AO-MM are generally smaller than those of our proposed method, which prevents the AO-MM from achieving a higher spectral efficiency.

VII. CONCLUSION

This paper considered the problem of joint beamforming for point-to-point RIS-assisted mmWave MIMO-OFDM systems. By exploiting the inherent structure of the mmWave effective channel, we established a mathematical relationship between the singular values of the effective channel and the reflection coefficients, based on which we developed a SVD approximation-based method for joint beamforming. An important advantage of the proposed method is that it can help achieve a desired channel by directly manipulating the singular

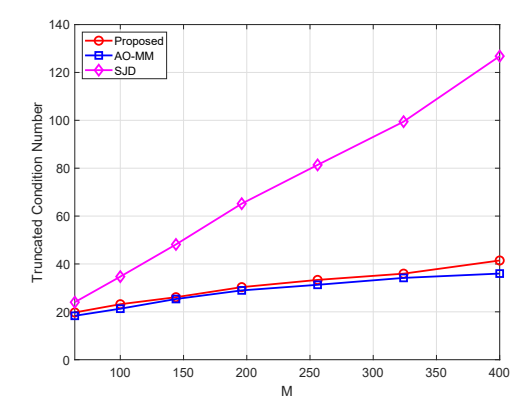


Fig. 7. Truncated condition number versus number of RIS elements M.

values of the effective channel. Simulation results shows that our proposed method can realize a favorable propagation channel with a small condition number, and achieve a clear performance advantage over existing methods.

REFERENCES

- T. S. Rappaport, J. N. Murdock, and F. Gutierrez, "State of the art in 60-ghz integrated circuits and systems for wireless communications," *Proc. IEEE*, vol. 99, no. 8, pp. 1390–1436, 2011.
- [2] S. Rangan, T. S. Rappaport, and E. Erkip, "Millimeter-wave cellular wireless networks: Potentials and challenges," *Proceedings of the IEEE*, vol. 102, no. 3, pp. 366–385, 2014.
- [3] A. Ghosh, T. A. Thomas, M. C. Cudak, R. Ratasuk, P. Moorut, F. W. Vook, T. S. Rappaport, G. R. MacCartney, S. Sun, and S. Nie, "Millimeter-wave enhanced local area systems: A high-data-rate approach for future wireless networks," *IEEE J. Sel. Areas Commun.*, vol. 32, no. 6, pp. 1152–1163, 2014.
- [4] A. L. Swindlehurst, E. Ayanoglu, P. Heydari, and F. Capolino, "Millimeter-wave massive MIMO: the next wireless revolution?" *IEEE Commun. Mag.*, vol. 52, no. 9, pp. 56–62, 2014.
- [5] O. Abari, "Enabling high-quality untethered virtual reality," in *Proc. 1st ACM Workshop Millim.-Wave Netw. Sens. Syst. (mmNets)*, ser. mmNets '17, New York, NY, USA, 2017, p. 49.
- [6] G. R. MacCartney, T. S. Rappaport, and S. Rangan, "Rapid fading due to human blockage in pedestrian crowds at 5g millimeter-wave frequencies," in *Proc. IEEE Global Commun. Conf. (GLOBECOM)*, 2017, pp. 1–7.
- [7] X. Tan, Z. Sun, D. Koutsonikolas, and J. M. Jornet, "Enabling indoor mobile millimeter-wave networks based on smart reflect-arrays," in *Proc. IEEE Conf. Comput. Commun. (INFOCOM)*, 2018, pp. 270–278.
- [8] P. Wang, J. Fang, X. Yuan, Z. Chen, and H. Li, "Intelligent reflecting surface-assisted millimeter wave communications: Joint active and passive precoding design," *IEEE Trans. Veh. Technol.*, vol. 69, no. 12, pp. 14960–14973, 2020.
- [9] N. S. Perović, M. D. Renzo, and M. F. Flanagan, "Channel capacity optimization using reconfigurable intelligent surfaces in indoor mmWave environments," in *Proc. IEEE Int. Conf. Commun. (ICC)*, 2020, pp. 1–7.
- [10] X. Yang, C.-K. Wen, and S. Jin, "MIMO detection for reconfigurable intelligent surface-assisted millimeter wave systems," *IEEE J. Sel. Areas Commun.*, vol. 38, no. 8, pp. 1777–1792, 2020.
- [11] C. Liaskos, S. Nie, A. Tsioliaridou, A. Pitsillides, S. Ioannidis, and I. Akyildiz, "A new wireless communication paradigm through softwarecontrolled metasurfaces," *IEEE Commun. Mag.*, vol. 56, no. 9, pp. 162– 169, 2018.
- [12] Y.-C. Liang, R. Long, Q. Zhang, J. Chen, H. V. Cheng, and H. Guo, "Large intelligent surface/antennas (LISA): Making reflective radios smart," J. Commun. Inf. Netw., vol. 4, no. 2, p. 11, 06 2019.
- [13] S. Hu, F. Rusek, and O. Edfors, "Beyond massive MIMO: The potential of data transmission with large intelligent surfaces," *IEEE Trans. Signal Process.*, vol. 66, no. 10, pp. 2746–2758, 2018.
- [14] E. Basar, M. Di Renzo, J. De Rosny, M. Debbah, M.-S. Alouini, and R. Zhang, "Wireless communications through reconfigurable intelligent surfaces," *IEEE Access*, vol. 7, pp. 116753–116773, 2019.

- [15] Q. Wu and R. Zhang, "Towards smart and reconfigurable environment: Intelligent reflecting surface aided wireless network," *IEEE Commun. Mag.*, vol. 58, no. 1, pp. 106–112, 2020.
- [16] Y. Han, W. Tang, S. Jin, C.-K. Wen, and X. Ma, "Large intelligent surface-assisted wireless communication exploiting statistical CSI," *IEEE Trans. Veh. Technol.*, vol. 68, no. 8, pp. 8238–8242, 2019.
- [17] Q. Wu and R. Zhang, "Intelligent reflecting surface enhanced wireless network: Joint active and passive beamforming design," in *Proc. IEEE Global Commun. Conf. (GLOBECOM)*, 2018, pp. 1–6.
- [18] C. Huang, A. Zappone, G. C. Alexandropoulos, M. Debbah, and C. Yuen, "Reconfigurable intelligent surfaces for energy efficiency in wireless communication," *IEEE Trans. Wireless Commun.*, vol. 18, no. 8, pp. 4157–4170, 2019.
- [19] Q. Wu and R. Zhang, "Intelligent reflecting surface enhanced wireless network via joint active and passive beamforming," *IEEE Trans. Wireless Commun.*, vol. 18, no. 11, pp. 5394–5409, 2019.
- [20] M. Cui, G. Zhang, and R. Zhang, "Secure wireless communication via intelligent reflecting surface," *IEEE Wireless Commun. Lett.*, vol. 8, no. 5, pp. 1410–1414, 2019.
- [21] B. Zheng and R. Zhang, "Intelligent reflecting surface-enhanced OFDM: Channel estimation and reflection optimization," *IEEE Wireless Commun. Lett.*, vol. 9, no. 4, pp. 518–522, 2020.
- [22] Y. Yang, B. Zheng, S. Zhang, and R. Zhang, "Intelligent reflecting surface meets OFDM: Protocol design and rate maximization," *IEEE Trans. Commun.*, vol. 68, no. 7, pp. 4522–4535, 2020.
- [23] K. Feng, X. Li, Y. Han, and Y. Chen, "Joint beamforming optimization for reconfigurable intelligent surface-enabled MISO-OFDM systems," *China Commun.*, vol. 18, no. 3, pp. 63–79, 2021.
- [24] B. Ning, Z. Chen, W. Chen, and J. Fang, "Beamforming optimization for intelligent reflecting surface assisted MIMO: A sum-path-gain maximization approach," *IEEE Wireless Commun. Lett.*, vol. 9, no. 7, pp. 1105–1109, 2020.
- [25] P. Wang, J. Fang, L. Dai, and H. Li, "Joint transceiver and large intelligent surface design for massive MIMO mmWave systems," *IEEE Trans. Wireless Commun.*, vol. 20, no. 2, pp. 1052–1064, 2021.
- [26] W. Chen, C.-K. Wen, X. Li, and S. Jin, "Channel customization for joint Tx-RISs-Rx design in hybrid mmWave systems," arXiv:2109.13058, Sept. 2021. [Online]. Available: https://arxiv.org/abs/2109.13058
- [27] R. Li, B. Guo, M. Tao, Y.-F. Liu, and W. Yu, "Joint design of hybrid beamforming and reflection coefficients in RIS-aided mmWave MIMO systems," *IEEE Trans. Commun.*, vol. 70, no. 4, pp. 2404–2416, 2022.
- [28] C. Feng, W. Shen, J. An, and L. Hanzo, "Joint hybrid and passive RIS-assisted beamforming for mmWave MIMO systems relying on dynamically configured subarrays," *IEEE IoT J.*, vol. 9, no. 15, pp. 13 913–13 926, 2022.
- [29] S. Zhang and R. Zhang, "Capacity characterization for intelligent reflecting surface aided MIMO communication," *IEEE J. Sel. Areas Commun.*, vol. 38, no. 8, pp. 1823–1838, 2020.
- [30] W. Jiang, B. Chen, J. Zhao, Z. Xiong, and Z. Ding, "Joint active and passive beamforming design for the IRS-assisted MIMOME-OFDM secure communications," *IEEE Trans. Veh. Technol.*, vol. 70, no. 10, pp. 10369–10381, 2021.
- [31] S. H. Hong, J. Park, S.-J. Kim, and J. Choi, "Hybrid beamforming for intelligent reflecting surface aided millimeter wave MIMO systems," *IEEE Trans. Wireless Commun.*, pp. 1–1, 2022.
- [32] A. Alkhateeb and R. W. Heath, "Frequency selective hybrid precoding for limited feedback millimeter wave systems," *IEEE Trans. Wireless Commun.*, vol. 64, no. 5, pp. 1801–1818, 2016.
- [33] X. Yu, J.-C. Shen, J. Zhang, and K. B. Letaief, "Alternating minimization algorithms for hybrid precoding in millimeter wave MIMO systems," *IEEE J. Sel. Areas Commun.*, vol. 10, no. 3, pp. 485–500, 2016.
- [34] Z. Gao, C. Hu, L. Dai, and Z. Wang, "Channel estimation for millimeterwave massive MIMO with hybrid precoding over frequency-selective fading channels," *IEEE Commun. Lett.*, vol. 20, no. 6, pp. 1259–1262, 2016.
- [35] P. Wang, J. Fang, H. Duan, and H. Li, "Compressed channel estimation for intelligent reflecting surface-assisted millimeter wave systems," *IEEE Signal Process. Lett.*, vol. 27, pp. 905–909, 2020.
- [36] J. He, H. Wymeersch, and M. Juntti, "Channel estimation for RIS-aided mmWave MIMO systems via atomic norm minimization," *IEEE Trans. Wireless Commun.*, vol. 20, no. 9, pp. 5786–5797, 2021.
- [37] Y. Liu, S. Zhang, F. Gao, J. Tang, and O. A. Dobre, "Cascaded channel estimation for RIS assisted mmWave MIMO transmissions," *IEEE Commun. Lett.*, vol. 10, no. 9, pp. 2065–2069, 2021.
- [38] X. Wei, D. Shen, and L. Dai, "Channel estimation for RIS assisted wireless communications part I: Fundamentals, solutions, and future

- opportunities," IEEE Commun. Lett., vol. 25, no. 5, pp. 1398-1402, 2021.
- [39] X. Zheng, P. Wang, J. Fang, and H. Li, "Compressed channel estimation for IRS-assisted millimeter wave OFDM systems: A low-rank tensor decomposition-based approach," *IEEE Wireless Commun. Lett.*, vol. 11, no. 6, pp. 1258–1262, 2022.
- [40] O. E. Ayach, S. Rajagopal, S. Abu-Surra, Z. Pi, and R. W. Heath, "Spatially sparse precoding in millimeter wave MIMO systems," *IEEE Trans. Wireless Commun.*, vol. 13, no. 3, pp. 1499–1513, 2014.
- [41] X. Gao, L. Dai, S. Han, C.-L. I, and R. W. Heath, "Energy-efficient hybrid analog and digital precoding for mmWave MIMO systems with large antenna arrays," *IEEE J. Sel. Areas Commun.*, vol. 34, no. 4, pp. 998–1009, 2016.
- [42] A. Goldsmith, S. Jafar, N. Jindal, and S. Vishwanath, "Capacity limits of MIMO channels," *IEEE J. Sel. Areas Commun.*, vol. 21, no. 5, pp. 684–702, 2003.
- [43] K. Alhujaili, V. Monga, and M. Rangaswamy, "Transmit mimo radar beampattern design via optimization on the complex circle manifold," *IEEE Trans. Signal Process.*, vol. 67, no. 13, pp. 3561–3575, 2019.
- [44] P.-A. Absil, R. Mahony, and R. Sepulchre, Optimization Algorithms on Matrix Manifolds. Princeton, NJ, USA: Princeton Univ. Press, 2007.
- [45] N. Boumal, P.-A. Absil, and C. Cartis, "Global rates of convergence for nonconvex optimization on manifolds," *IMA Journal of Numerical Analysis*, vol. 39, no. 1, pp. 1–33, 2019.
- [46] H. Kasai, "Fast optimization algorithm on complex oblique manifold for hybrid precoding in millimeter wave MIMO systems," in *Proc. IEEE Global Conf. Signal Inf. Process. (GlobalSIP)*, 2018, pp. 1266–1270.
- [47] B. Ning, Z. Chen, W. Chen, Y. Du, and J. Fang, "Terahertz multi-user massive MIMO with intelligent reflecting surface: Beam training and hybrid beamforming," *IEEE Trans. Veh. Technol.*, vol. 70, no. 2, pp. 1376–1393, 2021.
- [48] M. R. Akdeniz, Y. Liu, M. K. Samimi, S. Sun, S. Rangan, T. S. Rappaport, and E. Erkip, "Millimeter wave channel modeling and cellular capacity evaluation," *IEEE J. Sel. Areas Commun.*, vol. 32, no. 6, pp. 1164–1179, 2014.
- [49] M. K. Samimi, G. R. MacCartney, S. Sun, and T. S. Rappaport, "28 ghz millimeter-wave ultrawideband small-scale fading models in wireless channels," in *Proc. IEEE 83rd Veh. Technol. Conf. (VTC Spring)*, 2016, pp. 1–6.
- [50] H. Zhao, R. Mayzus, S. Sun, M. Samimi, J. K. Schulz, Y. Azar, K. Wang, G. N. Wong, F. Gutierrez, and T. S. Rappaport, "28 ghz millimeter wave cellular communication measurements for reflection and penetration loss in and around buildings in New York city," in *Proc. IEEE Int. Conf. Commun. (ICC)*, 2013, pp. 5163–5167.

Hanyu Wang received the B.Sc. degree from the inversity of electronic Science and Technology of China (UESTC), in 2016, where he has been working toward the Ph.D. degree since September 2018. His current research interests include compressed sensing, millimeter wave, and massive multipleinput and multiple-output (MIMO) communications.



Jun Fang (SM'19) received the B.S. and M.S. degrees from the Xidian University, Xi'an, China in 1998 and 2001, respectively, and the Ph.D. degree from the National University of Singapore, Singapore, in 2006, all in electrical engineering.

During 2006, he was a postdoctoral research associate in the Department of Electrical and Computer Engineering, Duke University. From January 2007 to December 2010, he was a research associate with the Department of Electrical and Computer Engineering, Stevens Institute of Technology. Since 2011, he has

been with the University of Electronic of Science and Technology of China, where he is currently a Professor. His research interests include compressed sensing and sparse theory, massive MIMO/mmWave communications, and statistical inference.

Dr. Fang was the recipient of the IEEE Jack Neubauer Memorial Award in 2013 for the best systems paper published in the *IEEE Transactions on Vehicular Technology*. He served as an Associate Technical Editor for *IEEE Communications Magazine* from 2012 to 2020. He is currently a Member of the IEEE SPS Sensor Array and Multichannel TC, and a Senior Associate Editor for *IEEE Signal Processing Letters*.



Hongbin Li (M'99-SM'08-F'19) received the B.S. and M.S. degrees from the University of Electronic Science and Technology of China, in 1991 and 1994, respectively, and the Ph.D. degree from the University of Florida, Gainesville, FL, in 1999, all in electrical engineering.

From July 1996 to May 1999, he was a Research Assistant in the Department of Electrical and Computer Engineering at the University of Florida. Since July 1999, he has been with the Department of Electrical and Computer Engineering, Stevens

Institute of Technology, Hoboken, NJ, where he is currently the Charles and Rosanna Batchelor Memorial Chair Professor. He was a Summer Visiting Faculty Member at the Air Force Research Laboratory in the summers of 2003, 2004 and 2009. His general research interests include statistical signal processing, wireless communications, and radars.

Dr. Li received the IEEE Jack Neubauer Memorial Award in 2013 from the IEEE Vehicular Technology Society, Outstanding Paper Award from the IEEE AFICON Conference in 2011, Provost's Award for Research Excellence in 2019, Harvey N. Davis Teaching Award in 2003, and Jess H. Davis Memorial Research Award in 2001 from Stevens Institute of Technology, and Sigma Xi Graduate Research Award from the University of Florida in 1999. He has been a member of the IEEE SPS Signal Processing Theory and Methods Technical Committee (TC) and the IEEE SPS Sensor Array and Multichannel TC, an Associate Editor for Signal Processing (Elsevier), IEEE Transactions on Signal Processing, IEEE Signal Processing Letters, and IEEE Transactions on Wireless Communications, as well as a Guest Editor for IEEE Journal of Selected Topics in Signal Processing and EURASIP Journal on Applied Signal Processing. He has been involved in various conference organization activities, including serving as a General Co-Chair for the 7th IEEE Sensor Array and Multichannel Signal Processing (SAM) Workshop, Hoboken, NJ, June 17-20, 2012. Dr. Li is a member of Tau Beta Pi and Phi Kappa Phi.